

Full paper

A high-performance sodium-ion battery enhanced by macadamia shell derived hard carbon anode



Yuheng Zheng^{a,b}, Yuesheng Wang^b, Yaxiang Lu^b, Yong-Sheng Hu^{b,*}, Ju Li^{a,c,*}

^a Frontier Institute of Science and Technology, Xi'an Jiaotong University, Xi'an 710049, China

^b Key Laboratory for Renewable Energy, Beijing Key Laboratory for New Energy Materials and Devices, Beijing National Laboratory for Condensed Matter Physics, Institute of Physics, Chinese Academy of Sciences, School of Physical Sciences, University of Chinese Academy of Sciences, Beijing 100190, China

^c Department of Nuclear Science and Engineering and Department of Materials Science and Engineering, MIT, Cambridge, MA 02139, USA

ARTICLE INFO

Keywords:

Hard carbon
Half-cell
Full-cell
Sodium-ion battery

ABSTRACT

Hard carbon anode materials for sodium-ion batteries (SIB) have usually been tested in half-cells by cycling between 0–2 V, and is believed to exhibit low rate capability. However, we find that the specific capacity, the rate performance, and the cycling performance may all be severely underestimated with the traditional half-cell cycling evaluation method, due to premature truncation of part II of the capacity (part I is “sloping”, part II is “plateauing”, while part III is Na metal deposition). Here we introduce a sodium-matched SIB full-cell architecture, with newly developed hard carbon derived from macadamia shell (MHC) as anode and Na[Cu_{1/9}Ni_{2/9}Fe_{1/3}Mn_{1/3}]O₂ (NCNFM) as the cathode material, with anode/cathode areal capacity ratio of 1.02–1.04. Our carefully balanced full-cells exhibit a cell-level theoretical specific energy of 215 Wh kg⁻¹ at C/10 and 186 Wh kg⁻¹ at 1C based on cathode-active and anode-active material weights, and an outstanding capacity retention of 70% after 1300 cycles (~2000 h). Traditional half-cell test (THT) of MHC using superabundant Na metal counter electrode shows only 51.7 mAh g⁻¹ capacity at 1C, and appears to die in no more than 100 h due to low open-circuit voltage slope and large polarization. A revised half-cell test (RHT) which shows much better agreements with full-cell test results, delivers a specific capacity of 314 mAh g⁻¹, with an initial Coulombic efficiency of ~91.4%, which is comparable to that of graphite anode in lithium-ion batteries.

1. Introduction

Lithium-ion batteries (LIB) are commercially successful due to high voltage, high cell-level energy density and long cycle life [1,2]. An appealing strategic alternative is sodium-ion batteries (SIB) [3–8], for the much greater abundance of sodium of about 23,000 ppm versus merely 17 ppm of highly unevenly distributed lithium in the Earth's crust. This has led to a price for Na₂CO₃ of about 50 times lower than Li₂CO₃. In addition, Al could be used as the negative current collector instead of Cu in SIB, and SIB full cell can be fully discharged in storage and transportation, which further reduce the cost.

There are already good choices of SIB cathode materials [9–19] with acceptable specific capacities and rate performances, but anode materials with large specific capacity, high initial Coulombic efficiency (ICE), and good rate performance are still lacking. Graphite, with an inter-planar spacing *d* of 0.34 nm, could not host Na [20,21]. Alloys [22–25], Ti-based oxides [26–32] and organic compounds [33–35] have also been explored but suffered from either a poor cycle life or a

low ICE, due to the large volume change during cycling or unstable chemistries. Disordered carbons, especially hard carbons (HC) [36–52], are the most promising anode materials for SIBs.

Usually, performances of the HCs, like the specific capacity, ICE, rate performance, and long-term cycling stability, are evaluated in a traditional half-cell test (THT) by cycling the cell between 0 V to ~2.0 V. Superabundant amount of Na metal is used as the counter electrode in THT, which has areal capacity with a heavy excess than that of the HC. This has two advantages:

1. Since HC will convert some cycleable Na⁺ into non-cycleable Na⁺ when forming solid-electrolyte-interphase (SEI), reflected by the Coulombic inefficiency (CI) [53], using superabundant Na counter electrode with a heavy excess at the beginning will remove the fear of running out of cycleable Na⁺.
2. If one were to use common cathode materials as the counter electrode to achieve superabundant reservoir, it will have to be very thick, and the electrical conduction could be a problem.

* Corresponding authors.

E-mail addresses: yshu@iphy.ac.cn (Y.-S. Hu), liju@mit.edu (J. Li).

URL: <http://li.mit.edu/> (J. Li).

<http://dx.doi.org/10.1016/j.nanoen.2017.07.018>

Received 11 June 2017; Received in revised form 4 July 2017; Accepted 10 July 2017

Available online 13 July 2017

2211-2855/ © 2017 Elsevier Ltd. All rights reserved.

Furthermore, standard cathode materials like $\text{Na}[\text{Cu}_{1/9}\text{Ni}_{2/9}\text{Fe}_{1/3}\text{Mn}_{1/3}]\text{O}_2$ (NCNFM) [9] can have significant open-circuit voltage (OCV) change with the material state of charge (SOC). Recall that OCV of a material can be hard to measure accurately in practice, since one not only needs to disconnect the circuit, but also needs to wait for a time period like in galvanostatic intermittent titration technique (GITT) until the voltage is fully relaxed. This waiting period is often many hours, even days. (Regarding the definition of SOC, in this paper we define a *cell* SOC Q in unit of mAh cm^{-2} , and a *material* SOC q in unit of $\text{mAh g}(\text{active})^{-1}$, where $g(\text{active})$ is the mass of the anode-active or cathode-active content without binder or conductive agents. We use Q in most derivations, because the cathode and anode experience the same $|\Delta Q|$, whereas q may budge much less for the same $|\Delta Q|$ if the mass loading ρ (unit $\text{g}(\text{active}) \text{cm}^{-2}$) of that electrode is superabundant: $Q = \rho q$.) But, bulk Na metal's OCV does not change with Q : $dU_{\text{Na}}^{\text{OCV}}(Q)/dQ = 0$, in reference to any standard reference electrode. If we use bulk Na metal itself as the reference electrode, then by definition $U_{\text{Na}}^{\text{OCV}}(Q) = 0 \text{ V}$.

In THT, one directly measures the potential difference $V_h(Q)$ between HC and bulk Na metal, but this protocol has its own problems, because half-cells of HC are intrinsically not so “robust” to polarization than most of the nearly-balanced full-cells using standard cathode materials, and can give nominally much worse “performance” for exactly the same HC electrode. This is somewhat counter-intuitive, since full-cell tests are more constrained (cycleable Na-constrained and electrolyte-constrained), but will be borne out by our analysis and experiments below.

To show this point conceptually, we note that ideally the configurations in half- and full-cells are basically the same, with the only difference in that the counter electrodes of superabundant Na metal are in the former while the cathode active materials, nearly balanced in areal capacity, are in the latter. Fig. 1a illustrates an ideally abstracted coin cell structure. Polarization would rise from all the phases (HC, SEI, electrolyte, and Na or CM (cathode material) and interfaces (I_a , I_b and I_c) involved. At a sodiation current density i

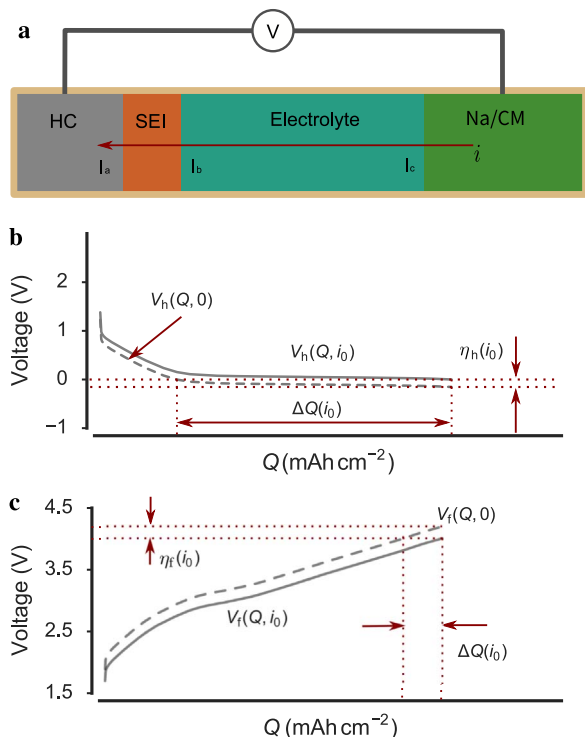


Fig. 1. Different robustness against polarization with half-cell and nearly-balanced full-cell. (a) The structures of the half-cell and the full-cell could be ideally abstracted as hard carbon cells with different counter electrode (Na or cathode materials), the schematic plots for the impact of polarization on the SOC at the end of sodiation process for (b) the half-cell and (c) the full-cell respectively. The slope of the full-cell is much larger than the half-cell, thus the full-cell could defeat more polarization.

$$i \equiv \frac{dQ}{dt} > 0, \quad (1)$$

assuming the total overpotential of the half- and full-cell are η_h and η_f , while U^{OCV} is dependent on Q (unit mAh cm^{-2}), η is dependent on Q and i , then at the same Q of HC, there are

$$V_h(Q, i) = U_{\text{HC}}^{\text{OCV}}(Q) - U_{\text{Na}}^{\text{OCV}}(Q) - \eta_h(Q, i) \quad (2)$$

for the half-cell test, and

$$V_f(Q, i) = U_{\text{CM}}^{\text{OCV}}(Q) - U_{\text{HC}}^{\text{OCV}}(Q) + \eta_f(Q, i) \quad (3)$$

for the full-cell test. (In this paper, we use V to denote cell voltages, and U^{OCV} to denote electrode voltages with respect to bulk Na metal reference. The sign of η is always positive, for any positive sodiation current i , half-cell or full-cell, to signify positive dissipation.) In above $U_{\text{HC}}^{\text{OCV}}$, $U_{\text{CM}}^{\text{OCV}}$ and $U_{\text{Na}}^{\text{OCV}}$ are the OCV of HC, cathode and Na respectively, and there is

$$U_{\text{Na}}^{\text{OCV}}(Q) = 0 \quad (4)$$

as previously discussed, Then we have

$$V_h(Q, i) = U_{\text{HC}}^{\text{OCV}}(Q) - \eta_h(Q, i) \quad (5)$$

$$V_f(Q, i) = U_{\text{CM}}^{\text{OCV}}(Q) - U_{\text{HC}}^{\text{OCV}}(Q) + \eta_f(Q, i). \quad (6)$$

in discharging of half-cell and charging of full-cell, at the same sodiation stage of HC.

Eqs. (5) and (6) reflect the voltage profile of the half-cell and the full-cell at different current density i . In THT, we define THT capacity as $Q_{\text{THT}} = |Q_{\text{VHighLimit}} - Q_{\text{VLowLimit}}|$ by voltage-cutoffs, and

$$\begin{aligned} \text{Half - cell: } V_{\text{HighLimit}} &= 2.5 \text{ V} \\ &\text{and } V_{\text{LowLimit}} = 0 \text{ V} \end{aligned} \quad (7)$$

$$\begin{aligned} \text{Full - cell: } V_{\text{HighLimit}} &= 4.0 \text{ V} \\ &\text{and } V_{\text{LowLimit}} = 1.5 \text{ V} \end{aligned} \quad (8)$$

As shown in Fig. 1b, $V_h(Q, 0)$ can get quite close to zero for large span of Q around the V_{LowLimit} (0 V), and there can be

$$\text{small } \left| \frac{dV^{\text{OCV}}(Q)}{dQ} \right|, \quad (9)$$

a plateauing cell-voltage slope near cutoff. This is the defining characteristic of vulnerable measurement systems, as demonstrated in Fig. 1b, and a large part of Q could be missed for the overpotential, which causes premature truncation of the sodiation process. Even if one does not use superabundant Na metal counter electrode, but use superabundant NCNFM (something like $3\times$ excess), a similar vulnerability could also arise. Note that this easily-missed Q range we are talking about could be highly reversible, physically speaking (underpotential deposition in inner, protected pores of HC, not true bulk metal deposition on outer surfaces of HC particles) and later proven by sodium-matched full-cell tests. They are just very vulnerable to be measured accurately due to polarization rise in THT.

Standard LIB cathodes like LiCoO_2 and SIB cathodes like NCNFM have significant voltage slopes with respect to its own material SOC q (unit mAh g^{-1}), so in a nearly Na-matched full-cell (not superabundant mass loading on cathode, in fact a bit cathode-deficient), as $Q = \rho q$ and ρ is constant in one specific cell, there will be significant

$$\left| \frac{dU_{\text{CM}}^{\text{OCV}}(Q)}{dQ} \right| \quad (10)$$

so even when $|dU_{\text{HC}}^{\text{OCV}}(Q)/dQ|$ gets small in the same Q range, the cell voltage will have

$$\text{significant } \left| \frac{dV^{\text{OCV}}(Q)}{dQ} \right|, \quad (11)$$

as demonstrated in Fig. 1c. So $|dV^{\text{OCV}}(Q)/dQ|$ of the sodium-matched full cell is much larger than that of the half cell, making the nearly Na-balanced full-cell test results much less vulnerable to overpotential interference and much more robust. As this work will show, there would be significant underestimation of reversible capacity with THT protocol if one uses a rigid sign truncation rule $V_{\text{LowLimit}} = 0$ V, as people usually do.

In addition, Na metal counter-electrode can actually induce quite a lot more impedance than expected. If we look into the polarization contributors of the half-cell and full-cell models carefully, the differences in impedance are introduced by the Na/cathode phase and the interface I_c . The ohmic drop across the cathode material (CM) phase in the full-cell is surely larger than the Na metal phase in the half-cell, but usually the cathode material in particle morphologies with dimensions of μm exhibits much larger electrochemically active area and consequently smaller Faradaic impedance at interface I_c , which could be more troublesome in the half-cells. As reported by Kasnatscheew et al. [54], ~60% of the capacity loss of the LIB NCM cathode in the first cycle could be recovered by a constant potential discharge process and the resulting lower ICE is mostly caused by kinetic inhibition of Li metal electrode. Moreover, they found that because the non-symmetric impedance of Li metal deposition and extraction from Li electrode, the cathode would exhibit an incomplete lithium retrieval every cycle, and thus leading to a rapid capacity fading [55]. This unfavorable character of Li metal electrode would cause more deviation in the investigation of the active materials at higher current density and is explained by Chen et al. [56], who observed the accumulated “dead lithium” covering the Li metal electrode. Analogous to the accumulating of “dead lithium”, the “dead Na” accumulation at the interface I_c is also highly problematic in half-cells, inducing continuously growing polarization.

Hence, HC reversible capacity may not be correctly characterized by THT. To definitely prove this, in this work we introduce a sodium-ion full-cell architecture, using newly developed hard carbon derived from direct pyrolysis of macadamia nut shell (MHC) as anode material, and $\text{Na}[\text{Cu}_{1/9}\text{Ni}_{2/9}\text{Fe}_{1/3}\text{Mn}_{1/3}]\text{O}_2$ (NCNFM) [9] as the cathode material. The Na-matched full cell (instead of superabundant half-cell) delivers a cell-level theoretical specific energy of 215 Wh kg^{-1} at C/10 based on anode-active and cathode-active material weights, and a capacity retention of 70% after 1300 cycles at 1C. To our knowledge, this is the most stable SIB full cell in cycle life ever achieved thus far [6]. With a newly suggested revised half-cell test (RHT) protocol, we find this MHC exhibits a specific capacity of 314 mAh g^{-1} with a THT ICE of 91.4%, which is comparable to the performance of graphite in LIBs. Importantly, we find that the full-cells are much more stable in cycling and with better rate performance than the traditional half-cells, as explained above. Hence we suggest that more attention should be paid to the performance of the active materials (cathode or anode) in the full-cell, rather than in the half-cell, configuration. Or at least, one should use the RHT protocol instead of the THT protocol in assessing the reversible capacity of hard carbons.

2. Experimental section

2.1. Material synthesis

The MHC samples were derived from direct pyrolysis of macadamia nut shell. In a typical process, 5 g of the smashed macadamia nut shell was carbonized for 2 h in a tube furnace under Argon flow. The pyrolysis temperatures were designed to be 1000 °C, 1200 °C, 1300 °C, 1400 °C, 1500 °C and 1600 °C respectively, and the as prepared samples were then marked as MHC1000, MHC1200, MHC1300, MHC1400, MHC1500 and MHC1600 respectively.

2.2. Material characterization

The structure was characterized by an X'Pert Pro MPD X-ray diffractometer (XRD) (Philips, Netherlands) using Cu – $K\alpha$ radiation (1.5405 Å). The morphologies of the samples were investigated with scanning electron microscope (SEM) (Hitachi S-4800). Transmission electron microscope (TEM) pictures were taken on a FEI Tecnai F20 transmission electron microscope. Nitrogen adsorption and desorption isotherms were determined on a Micromeritics ASAP 2020 analyzer.

2.3. Electrochemical measurements

All the electrochemical tests were conducted in CR2032 coin cells. MHC sample was mixed with sodium alginate with a weight ratio of 95:5, then deionized water was added to make slurry, which was subsequently coated on Al foil, to serve as anode for both half-cell and full-cell tests. The as-prepared electrodes were then dried at 120 °C in vacuum for 6 h. The mass loading of MHC was $\sim 2.0 \text{ mg cm}^{-2}$. A solution of 1 M NaPF_6 in ethylene carbonate (EC) and dimethyl carbonate (DMC) (1:1 in volume) with FEC (2%) to improve the SEI formation was utilized. Glass fiber was used as the separator. For the half-cells, sodium foil was used as the counter electrode. Full-cells was constructed with MHC1400 as the anode material and $\text{Na}[\text{Cu}_{1/9}\text{Ni}_{2/9}\text{Fe}_{1/3}\text{Mn}_{1/3}]\text{O}_2$ as the cathode material in a CR2032 cell. Synthesis method of the $\text{Na}[\text{Cu}_{1/9}\text{Ni}_{2/9}\text{Fe}_{1/3}\text{Mn}_{1/3}]\text{O}_2$ material was a conventional solid state reaction [9]. The procedure of making the cathode was the same as that of the anode, except for the slurry composition, which was 7:2:1 for the weight of the active material, super P, and PVDF. The capacity of the anode was designed to be 2–4% beyond the capacity of the cathode to avoid sodium metal deposition. The anodes and cathodes were cut to squares of $8 \text{ mm} \times 8 \text{ mm}$, and then assembled into coin cells. All the assembling operations were performed in the Argon-filled glove box. In the THT method, the half-cells were cycled in a voltage range between 0–2.5 V. The full-cells were cycled in a voltage range of 1.5–4.0 V at a current rate of C/10, C/2 and 1C.

The discharge and charge tests were carried out on a Land BT2000 battery test system (Wuhan, China) at room temperature.

3. Results and discussion

Before developing a new full-cell architecture, half-cells are usually assembled first to investigate the individual performance of the anode material and the cathode material, against a superabundant Na metal counter electrode. Most of the works on HCs are demonstrated in half-cells, providing the characters like specific capacity, ICE, rate performance and long term cycling stability [57,41,58,40,42]. The specific capacity is one of the most important parameters for a newly developed active material. ICE is another important characteristic, as it suggests how much SEI might form in the first cycle. High ICE, or low initial Coulombic inefficiency $\text{ICI} \equiv 1 - \text{ICE}$, is highly recommended for the development of anode materials for SIBs, for the low trapping ratio of active Na^+ in the first cycle and efficient use of the cathode material which provides the initial cyclable Na^+ inventory [53].

The specific capacity and ICE are traditionally derived from half-cell cycling between 0 V and ~ 2.0 V, assuming that the *material* SOC of HC when the instantaneous half-cell voltage $V_h(Q, i)$ reaches V_{LowLimit} (0 V) is the maximum reversible specific capacity that the HC could deliver. But as Section 1 explains, this is not necessarily true, especially when the overpotential gets large with current density i , and some of the highly reversible capacity (no Na metal plating on outer surface of HC particles) actually can occur at *negative* instantaneous half-cell voltage: $V_h(Q, i) < 0$ V.

We first performed THT in the half-cells. Just as Section 1 predicted, the rate performance and cycling performance are poor due to the rising polarization. Encouragingly, thanks to the low surface

area of MHC1400 as discussed in Section 3.1, the ICE achieved 91.4%, which is almost the level of graphite in lithium-ion batteries. Results of THT experiments, with voltage cutoff $V_{\text{LowLimit}}=0$ V are discussed in Section 3.2.

MHC1400 was then chosen for the Na-matched full-cell tests. The mass loadings of both electrodes, HC and NCNFM, were carefully designed to have nearly perfect matching areal capacity of ~ 0.6 mAh cm^{-2} , but with 2–4% excess of capacity on the anode side, to avoid over-sodiation in some part of the anode. In other words, the full-cell was made to be just slightly *cathode-deficient* to be on the safe side, avoiding Na dendrite deposition. The full-cells cycle stably and exhibit much better rate performance than the traditional half-cell tests, which is presented in Section 3.3. The Na-matched full cell delivers a cell-level theoretical specific energy of 215 Wh kg^{-1} at C/10, and 186 Wh kg^{-1} at 1C, based on cathode-active and anode-active material weights. The capacity retention is 70% after 1300 cycles at 1C, over ~ 2000 h. To our knowledge, this is the most stable SIB full cell in cycle life ever achieved [6].

Specific capacity of MHC1400 in the full-cell is surprisingly found to be larger than the specific capacity measured from the THT protocol, due to the polarization and rigid cutoff of instantaneous voltage $V_{\text{n}} = 0$ V in the THT. According to the analysis in Section 1, the real specific capacity is defined by when the *material* SOC of HC achieved the maximum reversible range. So we suggest an revised half-cell test (RHT) method to determine the real specific capacity in Section 3.4, and indeed obtain much larger values from RHT tests, in good agreement with full-cell test results in Section 3.3.

Hence we suggest a work-flow of designing a full-cell using just the first cycle of the THT result, without investigating the long-term cycling or rate performance of half-cells. The THT ICE could be derived in the first cycle, and then one can do over-discharge of the half-cell, to determine the real specific capacity in the RHT manner. Then, the full-cell could be designed by meticulously matching the areal capacity of cathode to the RHT areal capacity of HC, with a small deficiency on the cathode side.

3.1. Characterization of MHCs

Macadamia nutshell is biomass waste and a precursor of active carbon [59]. Being of low cost $\sim \$0.15$ kg^{-1} , it is suitable to be processed into hard carbon (MHC), with cost in scaled-up production estimated to be around $\$2$ kg^{-1} . The morphology of the MHC derived at the pyrolysis temperature of 1400 °C (MHC1400) was observed by SEM and TEM, as shown in Fig. 2a and b. The particle size is around 10 μm , and could be controlled by milling. A disordered atomic structure is revealed by the TEM image in Fig. 2b, which composes of small domains with 3–5 graphene layers, which are generally curved.

The previous report [60] has evaluated the impurity of the product of calcination by means of XPS, and found the hard carbon derived at 1400 °C is actually of quite high purity. We have also performed XPS examination on MHC1400, and the result and atomic percentage are shown as Fig. S1 and Table 1. The main impurity is Oxygen.

The XRD spectra characterize the structure of MHC formed at different pyrolysis temperatures, as shown in Fig. 2c. For an ideal graphite crystal, the XRD spectra would present some δ -functions along the angle axis, which represent different planes of the crystal. But the grain size effect would be significant if the crystal is in nano-scale, and the δ -functions would widen into bands with the decreased size of the crystal. Two broad bands could be observed in the XRD spectra of each sample, related to the (10 $\bar{1}$ 0) and (0002) planes of the nano graphitic crystals respectively. The (10 $\bar{1}$ 0) peak grows more and more sharper with the increase of the pyrolysis temperature, indicating that the “conjugated honey-comb” structure of the graphene is growing with the pyrolysis temperature. The position of (0002) peak shifts towards the right side and implies an interplanar spacing decreasing of the nano graphitic crystals, which is a structure relaxing towards the thermo-

dynamically stable state (ideal graphite crystal). For MHC1400, the interplanar spacing d is ~ 0.39 nm. According to DFT calculations [61], this interplanar spacing would facilitate the Na intercalation and de-intercalation through the graphene layers.

The BET surface area of porous materials from the N_2 absorption and desorption method is usually conducted to evaluate the electrochemically active area, especially for supercapacitor applications. Different from the electrical double layer (EDL) supercapacitors that favor large electrochemically active area, small values are preferred here due to the formation of SEI on the anode materials, which would trap the active Na^+ ions and could drive a sodium-constrained full-cell to “Na-exhaustion” (running out of cyclable Na^+). But this is not absolutely necessary, as high ICE may also be achieved using an ether-based electrolyte to form a stable, thin, compact and uniform SEI, as reported by Zhang et al. [62]. The BET surface area decreases with the increasing pyrolysis temperature, as Fig. 2d shows. We examined the in-pore surface area accumulation versus the pore size, and found that pores with width less than 1 nm contribute the major part of the surface area for MHC1000. With the increasing pyrolysis temperature, pores on the surface of HC disappears gradually from small ones to the larger ones, as presented in Fig. S2. This trend should give an increasing ICE, which will be shown in Section 3.4.

3.2. Traditional half-cell tests (THT) of MHC

Half-cell tests of a new anode or cathode material are usually provided first [38,40], in order to get basic parameters discussed above. But since the counter electrode is usually Na metal, there are certainly some differences to the condition when the active material is applied in full-cells. The Na metal counter electrode would consume the electrolyte continuously and form a lot of SEI [63,64] on the Na electrode surface, inducing “dead Na” accumulation and increasing the cell overpotential as Section 1 discussed. Especially for HC, which is most vulnerable to misinterpretation due to small $|dU_{\text{HC}}^{\text{OCV}}(Q)/dQ|$, its actual rate capability can be severely underestimated, i.e. “masked” by the over-potential caused by e.g. SEI on Na metal electrode. We also examined the cycling and rate performance of the MHC samples in half-cells and found that both the rate performance and the cycling performance of the THT protocol poorly reflect its actual performance in full cells, which initially sounds counter-intuitive since full-cells requires maintaining a delicate balance over many cycles.

Fig. 3 presents the THT performance of MHC. The peak first-cycle reversible specific capacity is observed from the half-cell of MHC1400, which is 300.9 mAh g^{-1} . The THT specific capacities of the samples increase with the pyrolysis temperature but decrease after 1400 °C. This trend has also been demonstrated in previous work [40,65], but we will show in Section 3.4 that this is an artificial result, caused by the rigid cut-off voltage of the discharging.

MHC1400 is chosen for investigation of the rate and cycling performance. Coincident with the predicted situation in Section 1, the rate performance in half-cells is very poor, with the specific capacity fading to just $\sim 17\%$ of that of C/10 at 1C, as shown in Fig. 3b. As Fig. 1c indicates, the plateauing part of the capacity is overly sensitive to the current density i . This is not what we will find in the full-cell tests, which we would provide in Section 3.3, that counter-intuitively shows much more robust and optimistic performance for exactly the same hard carbon material and electrode.

Cycling performance is generally conducted at a low current rate in half-cells. In this work cycling performance of MHC1400 is tested in half-cells at different current rates. As Fig. 3c presents, the half-cell cycles about 850 h at C/10, but deteriorates drastically with the increased current rate. Fig. S3 presents the degrading of voltage profiles at 1C. The rising of the start voltage of the charging profile indicates polarization increasing with the cycle number, and it is the rising polarization that causes the nominal capacity decay in THTs. As discussed in Section 1, Na metal electrode is even more reactive than Li

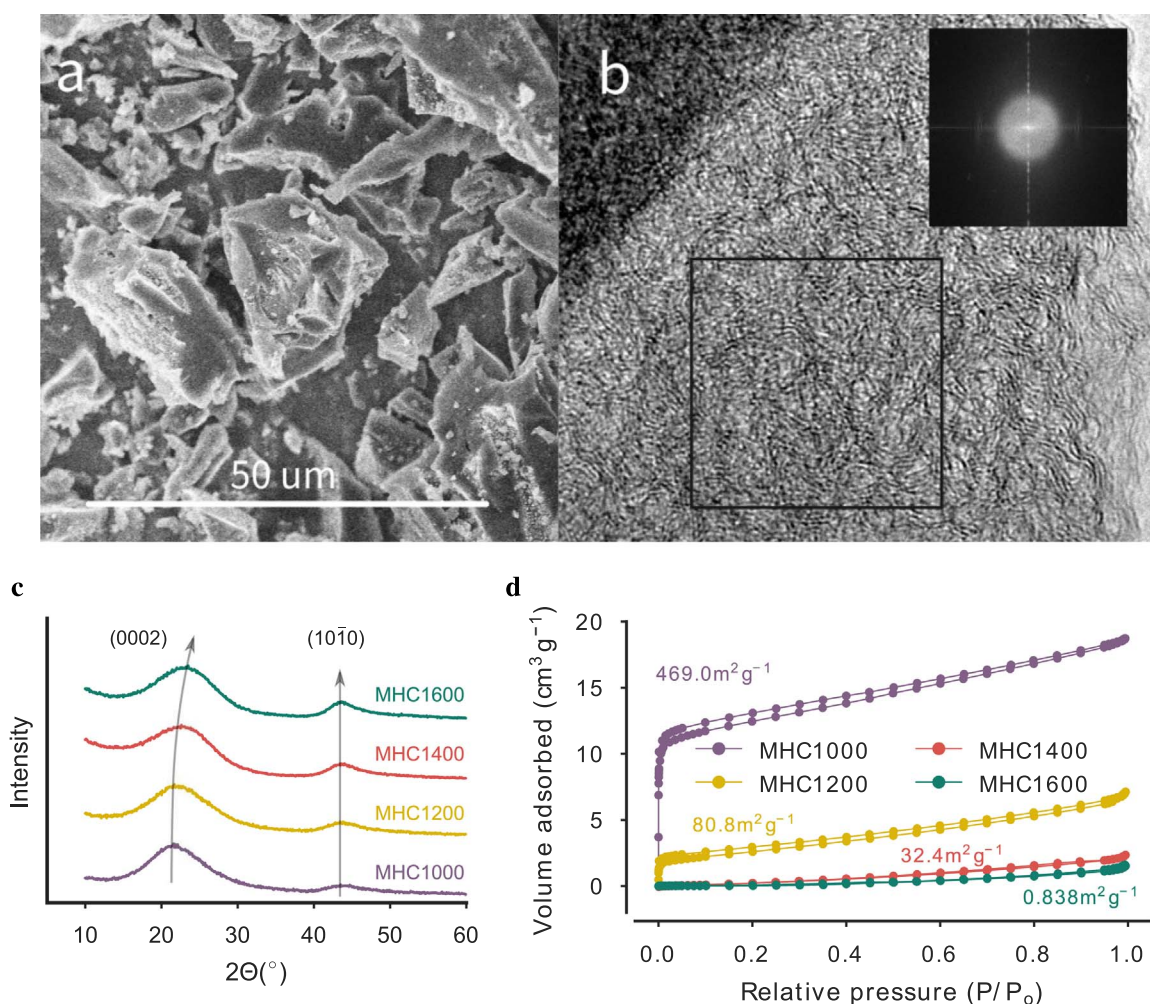


Fig. 2. Characterization of the MHCs. (a) The SEM image and (b) TEM image of MHC1400 with the corresponding FFT shown in the inset, (c) the XRD spectra, (d) N_2 adsorption-desorption isothermal results of MHC1000, MHC1200, MHC1400 and MHC1600.

Table 1
The atomic percentage of MHC1400 derived from XPS.

Element	C	O	N	K	Si	Cl
Atomic percentage / %	92.34	6.68	0.40	0.25	0.23	0.10

metal and should develop analogous structures as the “dead Na” and “Na flotsam” accumulation [64], and inducing more and more polarization. Meanwhile, the electrolyte is consumed by parasitic reactions with Na metal, and the half-cell finally dies with drying out of the electrolyte. The capacity fading versus cycle number was also plotted in Fig. S4. In Section 3.3, much better cycling performance of MHC1400 in full-cells will be delivered with carefully balanced NCNFM, which is not superabundant.

3.3. Full cell performance

With the poor THT rate performance and cycling data shown in Section 3.2, it seems discouraging to use MHC1400 for SIB anode. However, in this section, we will show that much more optimistic results could be achieved in Na-balanced full-cells.

Full cells adopting MHC1400 as the anode-active material and NCNFM as cathode-active material were assembled. The mass loadings of the MHC1400 and NCNFM is about 2 mg cm^{-2} and 6 mg cm^{-2} respectively, in roughly 1:3 ratio, according to their C/10 estimated capacity of 314 mAh g^{-1} (the real capacity, derived by an “observing V-

cusps” RHT manner in Section 3.4) and 118 mAh g^{-1} (2.5–4.0 V). The exact mass loading values of the anode and cathode for each specific cell were thus chosen as $(118 \times 1.02\text{--}1.04)$: (314), with a capacity excess of about 2–4% on the anode side, to avoid over-sodiation of the anode. The full-cells were cycled then between $V_f(Q, i) = 1.5\text{--}4.0 \text{ V}$ at current rates of C/10, C/2, and 1C respectively. Some characters of the full-cells and the performances are shown in Table 2 and Fig. 4.

Interestingly, the ICE or ICI is not solely determined by Na^+ trapping in SEI. For example, the ICE of the full-cell is 81.92%, with a specific discharge capacity of 297 mAh g^{-1} based on the actual anode-active content weight, which seems to indicate that the initial charge specific capacity should be 362.5 mAh g^{-1} , which however enormously exceeds the designed capacity of the NCNFM cathode. This implies that there must be some “fake” initial capacity or capacity loss, probably caused by redox of some soluble species in the electrolyte in the first cycle. So ICE of the full-cell could not serve as the exact indicator of how much Na^+ would be trapped in the SEI in the first cycle, and one should be careful in analyzing the derived capacity.

The THT specific capacity of 300.9 mAh g^{-1} is proved to be an underestimation. Assuming this 300.9 mAh g^{-1} is true, as the loading excess is 3.9% in this coin cell, the reported discharge capacity should maximally be (even without considering the limited Na source from cathode) only $300.9/(1 + 3.9\%) \approx 289.6 \text{ mAh g}^{-1}$, and is lower than the actual result. In this perspective, the THT method failed in the determination of the specific capacity of MHC1400, even with a slow test rate of C/10.

As Table 2 shows, specific capacity (SC) of the MHC1400 declined

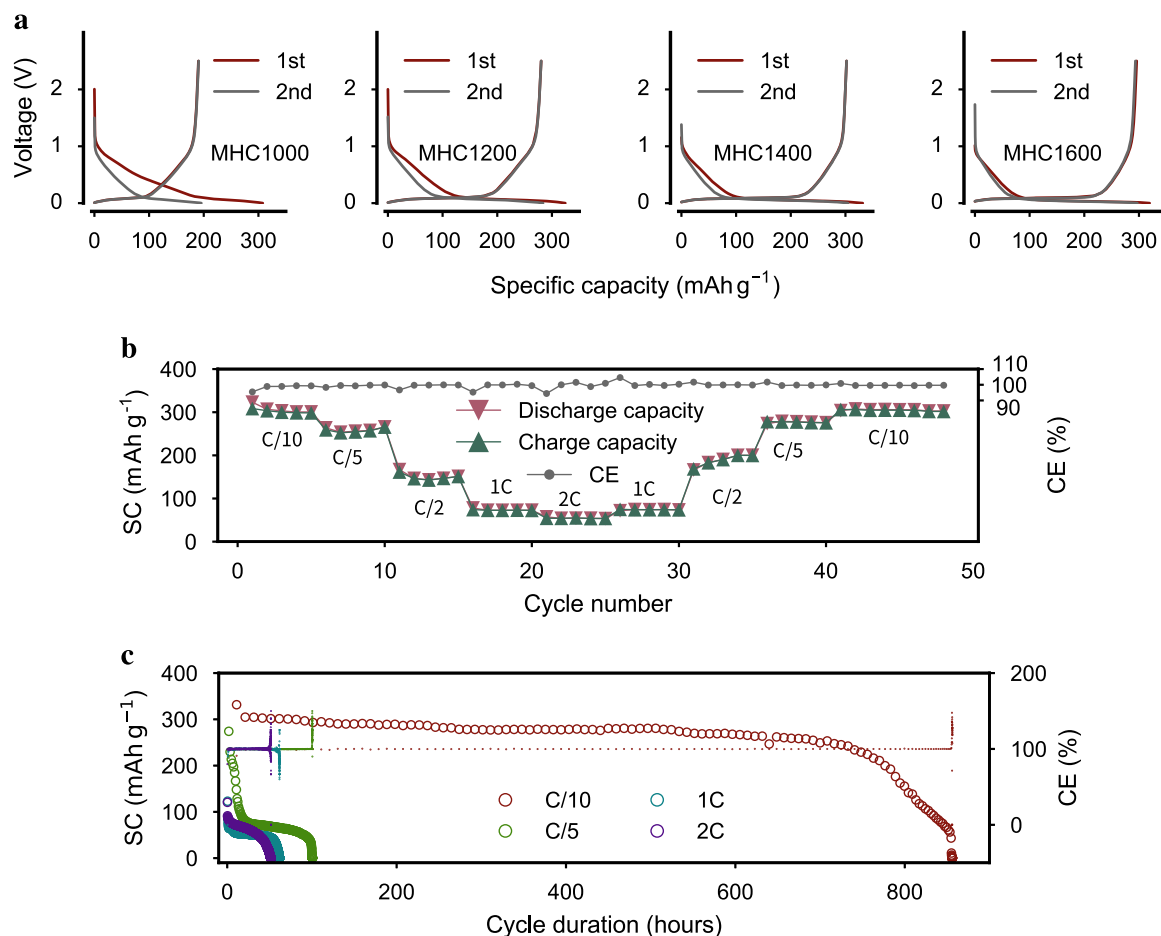


Fig. 3. Traditional half-cell test results. (a) Half cell cycling profile with samples derived from different temperature pyrolysis, (b) rate performance of the MHC1400 half-cell, (c) cycling performances of MHC1400 half-cell at different current rates.

Table 2

The full-cell performances at different C-rates.

C-rate	ICE/%	SC/ mAh g ⁻¹	SE/ Wh kg ⁻¹
C/10	81.92	297	215
C/2	84.31	274	197
1C	83.24	260	186

from 297 mAh g⁻¹ to 260 mAh g⁻¹ when the current rate increases to 1C in full-cell, which is 87.5% of the full-cell capacity at C/10. In contrast, the THT capacity at 1C is only ~17% of C/10 THT capacity, which further affirms the reasoning in Section 1.

With increasing C-rate, the theoretical specific energy¹ (SE) declined with an industrially acceptable rate in our Na-balanced full-cell tests. The SE at 1C is 186 Wh kg⁻¹ and is about 86.5% of that at C/10 (215 Wh kg⁻¹). The detailed rate performance of the Na-balanced full-cell is presented in Fig. 4d, and is much better than the THT performance presented in Fig. 3b.

The full-cell voltage profiles at the current rate of C/10 and 1C are shown in Fig. 4a and b respectively. Polarization is not significantly larger at 1C compared with that at C/10. After 1300 cycles at 1C as Fig. 4b presents, polarization grows enormously.

Our full-cell cycling performance is very stable as Fig. 4e shows (the cycling performance is also provided as specific capacity of cathode

versus cycle number in Fig. S5). Only 30% capacity fade is observed after 1300 cycles at 1C. Interestingly, we then set the current rate to C/10, and the specific capacity recovered to 252 mAh g⁻¹, corresponding to ~85% of the initial specific capacity at C/10 (297 mAh g⁻¹). This means that in the duration of this 1C cycling, about half of the capacity decay (15% out of 30%) is caused by active materials degradation, with the other half caused by increasing polarization. The total cycling duration exceed 2020 h (84 days) for this 70% capacity retention ratio (similar capacity retention ratio after 2030 h at C/2, shown in Fig. S6). Compared with Fig. 3c, in which the THT half-cells appear to die in no more than 100 h at the same current rate of 1C, one can find that the full-cell is benefiting much from the absence of Na metal electrode. This is indeed encouraging, as HC in half-cells may exhibit very crappy results, but there is still potential for it to achieve great performances in full-cells.

The full-cell above is just the first test. We then fabricated a cathode with a much larger NCNFM loading of 9.5 mg cm⁻² (93% of the total cathode mass loading), and to match with it, an anode with MHC1400 loading of ~3.1 mg cm⁻². To prevent Na metal deposition on the rim of anode at high current density, the cathode was made in a round shape with a diameter of 12 mm, and the anode was also in round shape but with a diameter of 14 mm (slightly larger than the cathode, to make sure that the anode area covers all the cathode area). This full-cell with industrially significant areal capacity (~1 mAh cm⁻²) was then cycled at 2C. The cycling performance is shown in Fig. S7 and the voltage profile is shown in Fig. 4c. After 300 cycles, the cell capacity faded just ~13%. We suspect this gentle capacity fading is caused by the side reaction between the electrolyte and the freshly deposited Na metal. Since the current density is certainly not uniform over all the area of the anode,

¹ The specific energy is calculated as $SE \equiv \frac{\int_0^{q_{dis}} V_{dq}}{m_{anode} + m_{cathode}}$, where q_{dis} denotes for the discharge capacity of one specific cycle, m_{anode} and $m_{cathode}$ denotes the weight of anode active material and cathode active material respectively.

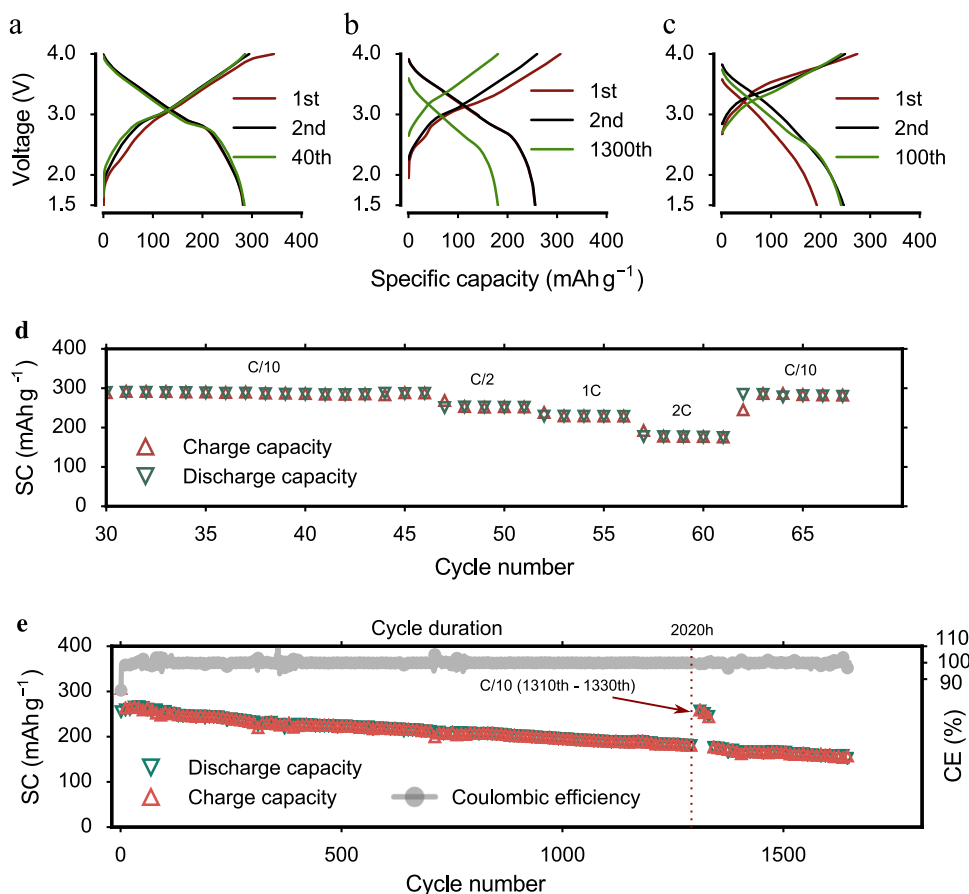


Fig. 4. Full-cell performance. Charge/Discharge profiles at the current rate of (a) C/10, (b) 1C and (c) 2C, (d) the rate performance, and (e) the cycling performance at 1C of the full-cell adopting MHC1400 as anode material and NCNFM as cathode material. The mass loadings were about $\sim 2 \text{ mg cm}^{-2}$ and $\sim 6 \text{ mg cm}^{-2}$ for the anode and cathode respectively, except for the full-cell cycled at 2C, which were $\sim 3.1 \text{ mg cm}^{-2}$ and $\sim 9.5 \text{ mg cm}^{-2}$ respectively and the anode is slightly larger in area than the cathode. Since the anode is with a heavy excess in capacity than the cathode, the specific capacity is calculated as $SC = SC_{\text{NCNFM}} \times AC_{\text{NCNFM}}/AC_{\text{MHC}}$, where SC_{NCNFM} denotes for the specific capacity of the cathode, AC_{NCNFM} and AC_{MHC} denotes for the areal capacity of the NCNFM cathode and MHC anode respectively.

there must be some part where the current density is larger than the expected values, thus inducing Na metal deposition in some part of the anode, resulting in a tiny degradation per cycle, which would be more significant with the increasing of the current density. But, as this is not the limitation of the material but that of the geometry, we believe the cycle life would be even more optimistic if larger-area anode used in industry was applied.

3.4. Determination of the real specific capacity with RHT

Cell-level specific energy is the key to any full-cell architecture [66], and the areal capacities of the anode and cathode must be carefully matched in the crafted full-cell to avoid redundancy and waste of active materials. Hence, the specific capacity of the anode and cathode materials need to be estimated before designing the anode and cathode mass loadings in the full-cell. Usually, specific capacity of anode/cathode material is derived from half-cell cycling, in which superabundant Na metal is used as the counter electrode. In THT, by cycling the half-cell between rigid voltage cutoffs, Eq. (7), the specific capacity is identified as $Q_{\text{THT}} = |Q_{2.5\text{V}} - Q_{0\text{V}}|$, as Fig. 3a shows. But in Section 3.3, one can find that the MHC1400 in full-cells achieved much higher specific capacity than in the half-cells, thus THT is actually underestimating the reversible capacity.

According to Eq. (5), THT is triggered by

$$U_{\text{HC}}^{\text{OCV}}(Q_{\text{VLowLimit}}) = \eta_{\text{h}}(Q_{\text{VLowLimit}}, i) > 0 \quad (12)$$

and since $i \uparrow$, $\eta_{\text{h}}(Q_{\text{VLowLimit}}, i) \uparrow$ sharply for high-polarization system, Eq. (12) indicates that the material SOC of the anode would decrease with

increasing of sodiation current density i , when the half-cell hits the rigid voltage cutoff V_{LowLimit} (0 V). So the specific capacity could be severely underestimated in half-cells, if the slope is too small

$$|dU_{\text{HC}}^{\text{OCV}}/dQ| \text{ too small, } U_{\text{HC}}^{\text{OCV}} > 0 \text{ Volt but small} \quad (13)$$

as Fig. 1b shows. And this situation would be more serious at higher current. This means the THT method may severely underestimate the part of the capacity that satisfies (13), especially at high current density i , even though that part of the capacity could be highly reversible as Section 3.3 proved.

To achieve a more reasonable determination of reversible capacity of HCs, we note that during sodiation, HC shows three stages in its sodiation capacity Q , as shown in Fig. S8. Part I has a large $|dU_{\text{HC}}^{\text{OCV}}/dQ|$:

$$\text{part I: } U_{\text{HC}}^{\text{OCV}} \text{ large, } |dU_{\text{HC}}^{\text{OCV}}/dQ| \text{ large} \quad (14)$$

and so is called the “sloping” stage, followed by part II which has a much smaller $|dU_{\text{HC}}^{\text{OCV}}/dQ|$, called the “plateauing” stage. Part II physically corresponds to underpotential deposition (UPD), where monolayers of metal atoms are deposited on a complete-wetting substrate, most likely some protected inner pore surfaces of HC, with energetics more favorable than depositing metal atoms onto the metal itself. In underpotential deposition of metals, the OCV is small but positive:

$$\text{part II: } 1\text{Volt} \gg U_{\text{HC}}^{\text{OCV}} > 0\text{Volt, } |dU_{\text{HC}}^{\text{OCV}}/dQ| \text{ small.} \quad (15)$$

Thus part II of the capacity satisfies (13) and is most vulnerable to polarization. However part II is actually reversible, because the UPD Na monolayers are inside the hermetic pores of HC, not in direct contact with the liquid electrolyte, and sealed off by the SEI on outer

surface of HC particles. Despite their low voltage (which is good from energy density point of view), they are of different physical origin from the Na metal dendrites (part III) that grows on the outer surface of HC particles, breaking SEIs and constantly reacting with the liquid electrolyte [64].

After part II, there is also part III, with the truly Na metal plating and dendritic growth on the outer surface of HC, with

$$\text{part III: } \frac{dV_h^{\text{OCV}}}{dQ} = \frac{dU_{\text{HC}}^{\text{OCV}}}{dQ} = 0. \quad (16)$$

This part is well-known to be *irreversible*, due to reaction between the Na metal and the liquid electrolyte [64]. Once part III occurs, a significant fraction of those additional sodium that one plates on the outer surface of HC particles cannot be pulled out ever again, forming “dead Na” and “Na flotsams” [64]. This reaction also causes liquid electrolyte dryout. Part III is a regime where a sodium-limited and electrolyte-limited full-cell definitely wants to avoid, in order to achieve industrially acceptable cyclability (like the 1300 cycles in Section 3.3). However, if one uses a rigid voltage cutoff criterion and just look at the magnitude of V_h at any given snapshot time, it is very hard to separate part II and part III. One tends to be overly conservative in THT, and “throws out the baby with the bathwater” with criterion (5) and (7).

Fortunately, when we look at the $V_h(Q, i)$ profile carefully into the slightly-negative voltage value regime, there is a “V” shaped cusp on the voltage profile demarcating Part II from Part III, which is caused by the Na metal nucleation barrier and indicates *material* SOC of HC achieves the max reversible specific capacity. Part I and Part II capacities of HCs are highly reversible even when some part could be slightly under 0 V in half-cells, as shown in Section 3.3, and could be defined as the real reversible specific capacity (sloping + UPD, but not bulk Na metal deposition on the outer surface of HC, which constantly breaks the fragile SEI and causes Na loss [64]).

Thus, we have come up with a “revised half-cell test” (RHT) protocol, where one discharges the half-cell till the Na metal deposition (part III) occurs after the “V”-cusp feature, then define the specific capacity right before the “V” cusp as the real specific capacity, or RHT capacity. In this “revised half-cell test”, after cycling 3 times with THT protocol with still superabundant Na metal counter electrode, the half-cells were then over-discharged, and a Na metal plating profile could be observed, as shown in Fig. 5a. One then locates the “V”-cusp feature in $V_h(Q, i)$, and define the RHT capacity as the capacity right before the “V”-cusp. The claim is that RHT capacity is actually highly reversible, matching well with what we can obtain in sodium-constrained and electrolyte-constrained, nearly perfectly-balanced full cells.

The THT and RHT specific capacities are plotted in Fig. 5b, along with the THT ICE. It can be seen in Fig. 5a that with the increase of the pyrolysis temperature, part I has a declining voltage and gradually shortened even though the slopes are approximately the same. The voltage of part II decreases with the rising of pyrolysis temperature, and thus is more and more sensitive to polarization. The real capacity of the sample continuously increases with pyrolysis temperature in the range of 1000 °C to 1600 °C. Interestingly, the “V”-cusp grows broader and broader, and nearly disappears for MHC1600. But using the point of the most abrupt change in slope

$$\Delta \frac{dV_h(Q, i)}{dQ} \quad (17)$$

still allows us to determine the separation between part II and part III.

While the THT capacity decreases from MHC1400 to MHC1600, it is likely just a testing artifact, and the observed decrease is actually induced by the large polarization (note the intercepts with the 0 V axis of the profile). We believe RHT is much more reliable to evaluate the real specific capacity of HCs than THT.

As shown in Fig. 5b, MHC1400 provides RHT capacity of 314 mAh g⁻¹ (with a THT ICE of 91.4%), and this number is actually

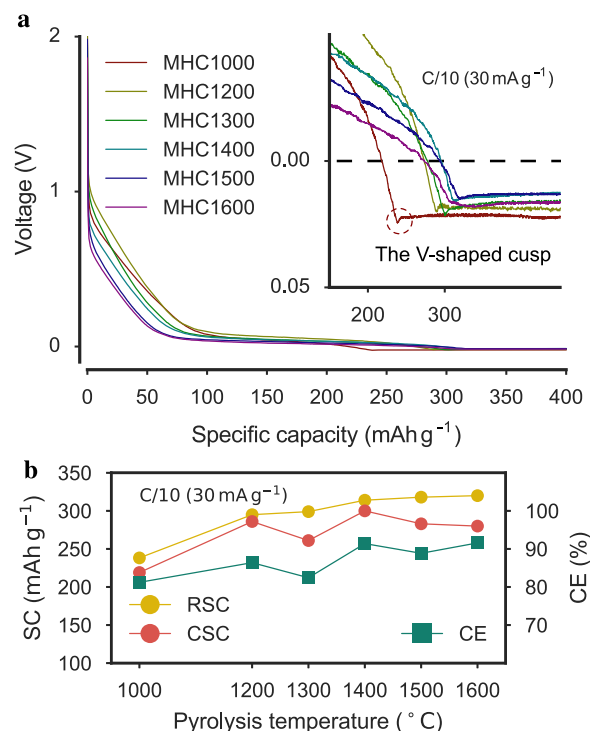


Fig. 5. (a) The deposition method of evaluating the real capacity and (b) the comparison of the RHT capacities and THT capacities.

used for the full-cell design. Although MHC1600 provides a little higher specific capacity of ~320 mAh g⁻¹, the plateau part of the voltage profile is lower, which induces more Na metal deposition risk than that of MHC1400.

The THT first cycle is still necessary to evaluate the ICE, which may help us understand the irreversible consumption of cycleable Na⁺ in the first cycle of the full-cell. As shown in Fig. 5b, the ICE increases to 91.4% at a pyrolysis temperature of 1400 °C, and becomes constant as the pyrolysis temperature rises. This ICE is similar to the graphite performance in LIBs, and is beneficial to the specific energy of the full-cell as Section 3.3 shows. Note, however, that the Coulombic Inefficiency (CI $\equiv 1 - \text{CE} \approx 8.6\%$) may be not completely induced by the irreversible Na⁺ trapping mechanism [53]. CI may also be induced by over-estimation of the first cycle sodiation capacity caused by the FEC decomposition [67], which is more explicit in the Na-constrained full cell test as discussed in Section 3.3. The decomposition of FEC generally occurs at 0.7 V vs. Na in the first discharge process of the half-cell, and this effect could be observed in Fig. 3a. And as shown in Section 3.3, the actually reversible capacity is 98.3% of the designed value (98.3% = 297/302.2, where 302.2 = 314/1.039), which indicates that there can only be 1.7% or less of the active Na⁺ trapped in SEI on the HC surface in the first cycle, as we are cathode-deficient to start with, and there are other electrode deprecation mechanisms in parallel like loss of electrical contact [53]. So here we have a stunning factor of 5 difference between the initial Coulombic Inefficiency (ICI) prediction (~8.6%) and the actual capacity decay (1.7%) in our well-balanced, slightly cathode-deficient full cell. Thus, ICI / CIC (Coulombic inefficiency cumulant) analysis [68,53] from the half-cell test is indicative, but not exact (can be *overpessimistic*) indicator of the cyclable Na⁺ inventory loss in the first cycle and beyond. This effect has also been observed in advanced LIB anodes [68], but the differences were smaller, and is attributed to soluble redox species in the liquid electrolyte [53]. It seems that in SIB full-cells with hard carbon anode, this difference between CIC prediction and the actual capacity fade is larger than the LIB full-cells. In other words, one should not be discouraged as *much* as by what the industrial lore “one needs >99.9% Coulombic Efficiency for a full cell to cycle 200 times” asserts [53].

Since the rate and cycling performances of the half-cell are actually

much worse than the in full-cells, due to impedance growth and electrolyte consumption on the Na metal counter electrode, we suggest that it is *unnecessary* to investigate half-cell rate performance and long-term cycling of HC materials in detail. Instead, one should directly proceed to test the full cells once ICE and the real specific capacity are derived from a few cycles of THT, followed by over-discharging of the half cell to determine the RHT capacity. The true rate performance and cyclability of new anode materials are better reflected when put against well-balanced amount of NCNFM, rather than superabundant amount of Na metal (which is “fictitious” from a practical standpoint anyway).

4. Conclusions

In summary, we have developed a new type of hard carbon from the direct pyrolysis of macadamia nut shell, with an ICE of 91.4% and real specific capacity of 314 mAh g⁻¹. The full-cell using MHC1400 and NCNFM as anode and cathode materials delivers a specific energy of 215 Wh kg⁻¹ based on the weight of the anode-active and cathode-active contents (HC+NCNFM). 70% of the capacity is still retained after cycling for 1300 cycles at 1C, spanning ~2000 hours, which is the most stable SIB full cell as far as we know. Most importantly, we found that the specific capacity is underestimated by the traditionally half-cell test, and suggest a revised half-cell test to determine the real specific capacity. The rate and long cycling performance of the MHC1400 in half-cells are much worse than those in the full-cells, and we suggest that one should pay more attention to the performance of full-cells, and one should be suspicious of the rate performance and cycling performance of the half-cells using superabundant Na. Finally, our full-cell tests show that the actual capacity decay and cyclable Na inventory loss is *much more optimistic* than what the Coulombic inefficiency cumulant (CIC) analysis tells us, by a factor of 5. This factor of discrepancy seems to be significantly larger than for LIBs.

Acknowledgments

This work was supported by funding from NSF ECCS-1610806, the National Key Technologies R & D Program (No. 2016YFB0901504) and National Natural Science Foundation of China (Nos. 51421002).

Appendix A. Supplementary data

Supplementary data associated with this article can be found in the online version at <http://dx.doi.org/10.1016/j.nanoen.2017.07.018>.

References

- [1] M. Armand, J.-M. Tarascon, Building better batteries, *Nature* 451 (2008) 652–657.
- [2] J.-M. Tarascon, Is lithium the new gold?, *Nat. Chem.* 2 (2010) 510.
- [3] N. Yabuuchi, K. Kubota, M. Dahbi, S. Komaba, Research development on sodium-ion batteries, *Chem. Rev.* 114 (2014) 11636–11682.
- [4] H. Kang, Y. Liu, K. Cao, Y. Zhao, L. Jiao, Y. Wang, H. Yuan, Update on anode materials for Na-ion batteries, *J. Mater. Chem. A* 3 (2015) 17899–17913.
- [5] H. Kim, H. Kim, Z. Ding, M.H. Lee, K. Lim, G. Yoon, K. Kang, Recent progress in electrode materials for sodium-ion batteries, *Adv. Energy Mater.* 6 (2016) 1600943.
- [6] W. Ren, Z. Zhu, Q. An, L. Mai, Emerging prototype sodium-ion full cells with nanostructured electrode materials, *Small* (2017) 1604181.
- [7] Y. Li, Y. Lu, C. Zhao, Y.S. Hu, M.M. Titirici, H. Li, X. Huang, L. Chen, Recent advances of electrode materials for low-cost sodium-ion batteries towards practical application for grid energy storage, *Energy Storage Mater.* 7 (2017) 130–151.
- [8] J. Cui, S. Yao, J.K. Kim, Recent progress in rational design of anode materials for high-performance Na-ion batteries, *Energy Storage Mater.* 7 (2017) 64–114.
- [9] L. Mu, X. Qi, Y.S. Hu, H. Li, L. Chen, X. Huang, Electrochemical properties of novel O3-NaCu1/9Ni2/9Fe1/3Mn1/3O2 as cathode material for sodium-ion batteries, *Energy Storage Sci. Technol.* 5 (3) (2016) 324–328.
- [10] L. Mu, S. Xu, Y. Li, Y.S. Hu, H. Li, L. Chen, X. Huang, Prototype sodium-ion batteries using an air-stable and Co/Ni-free O3-layered metal oxide cathode, *Adv. Mater.* 27 (2015) 6928–6933.
- [11] R. Kataoka, T. Mukai, A. Yoshizawa, T. Sakai, Development of high capacity cathode material for sodium ion batteries Na0.95Li0.15(Ni0.15Mn0.55Co0.1)O2, *J. Electrochem. Soc.* 160 (2013) A933–A939.
- [12] J. Billaud, G. Singh, A.R. Armstrong, E. Gonzalo, V. Roddatis, M. Armand, T. Rojo, P.G. Bruce, Na0.67Mn1xMgxO2 (0 < x < 0.2): a high capacity cathode for sodium-ion batteries, *Energy Environ. Sci.* 7 (2014) 1387.
- [13] S.M. Oh, S.T. Myung, J.Y. Hwang, B. Scrosati, K. Amine, Y.K. Sun, High capacity O3-type Na[Li0.05(Ni0.25Fe0.25Mn0.5)0.95]O2 cathode for sodium ion batteries, *Chem. Mater.* 26 (2014) 6165–6171.
- [14] S.-Y. Xu, X.-Y. Wu, Y.-M. Li, Y.-S. Hu, L.-Q. Chen, Novel copper redox-based cathode materials for room-temperature sodium-ion batteries, *Chin. Phys. B* 23 (2014) 118202.
- [15] N. YABUUCHI, H. YOSHIDA, S. KOMABA, Crystal structures and electrode performance of alpha-NaFeO2 for rechargeable sodium batteries, *Electrochemistry* 80 (2012) 716–719.
- [16] P. Vassilaras, X. Ma, X. Li, G. Ceder, Electrochemical properties of monoclinic NaNiO2, *J. Electrochem. Soc.* 160 (2012) A207–A211.
- [17] S. Komaba, C. Takei, T. Nakayama, A. Ogata, N. Yabuuchi, Electrochemical intercalation activity of layered NaCrO2 vs. LiCrO2, *Electrochem. Commun.* 12 (2010) 355–358.
- [18] X. Ma, H. Chen, G. Ceder, Electrochemical properties of monoclinic NaMnO2, *J. Electrochem. Soc.* 158 (2011) A1307.
- [19] C. Fang, Y. Huang, W. Zhang, J. Han, Z. Deng, Y. Cao, H. Yang, Routes to high energy cathodes of sodium-ion batteries, *Adv. Energy Mater.* 6 (2016) 1501727.
- [20] P. Ge, M. Foulletier, Electrochemical intercalation of sodium in graphite, *Solid State Ion.* 28–30 (1988) 1172–1175.
- [21] Y. Wen, K. He, Y. Zhu, F. Han, Y. Xu, I. Matsuda, Y. Ishii, J. Cumings, C. Wang, Expanded graphite as superior anode for sodium-ion batteries, *Nat. Commun.* 5 (2014) 4033.
- [22] L. Xiao, Y. Cao, J. Xiao, W. Wang, L. Kovarik, Z. Nie, J. Liu, High capacity, reversible alloying reactions in SnSb/C nanocomposites for Na-ion battery applications, *Chem. Commun.* 48 (2012) 3321.
- [23] Y. Xu, Y. Zhu, Y. Liu, C. Wang, Electrochemical performance of porous carbon/tin composite anodes for sodium-ion and lithium-ion batteries, *Adv. Energy Mater.* 3 (2013) 128–133.
- [24] J. Qian, X. Wu, Y. Cao, X. Ai, H. Yang, High capacity and rate capability of amorphous phosphorus for sodium ion batteries, *Angew. Chem. - Int. Ed.* 52 (2013) 4633–4636.
- [25] Y. Xu, E. Swaans, S. Basak, H.W. Zandbergen, D.M. Borsa, F.M. Mulder, Reversible Na-ion uptake in Si nanoparticles, *Adv. Energy Mater.* 6 (2016) 1501436.
- [26] Y. Wang, X. Yu, S. Xu, J. Bai, R. Xiao, Y.S. Hu, H. Li, X.Q. Yang, L. Chen, X. Huang, A zero-strain layered metal oxide as the negative electrode for long-life sodium-ion batteries, *Nat. Commun.* 4 (2013) 2365.
- [27] L. Zhao, H.-L. Pan, Y.-S. Hu, H. Li, L.-Q. Chen, Spinel lithium titanate (Li₂Ti₂O₁₂) as novel anode material for room-temperature sodium-ion battery, *Chin. Phys. B* 21 (2012) 028201.
- [28] H. Pan, X. Lu, X. Yu, Y.-S. Hu, H. Li, X.-Q. Yang, L. Chen, Sodium storage and transport properties in layered Na₂Ti₃O₇ for room-temperature sodium-ion batteries, *Adv. Energy Mater.* 3 (2013) 1186–1194.
- [29] S.K. Panday, B. Jache, H. Lahon, C.L. Bender, J. Janek, P. Adelhelm, Graphene mediated improved sodium storage in nanocrystalline anatase TiO₂ for sodium ion batteries with ether electrolyte, *Chem. Commun.* 52 (2016) 1428–1431.
- [30] H. Xiong, M.D. Slater, M. Balasubramanian, C.S. Johnson, T. Rajh, Amorphous, TiO₂ nanotube anode for rechargeable sodium ion batteries, *J. Phys. Chem. Lett.* 2 (2011) 2560–2565.
- [31] J. Chen, Y. Zhang, G. Zou, Z. Huang, S. Li, H. Liao, J. Wang, H. Hou, X. Ji, Size-tunable olive-like anatase TiO₂ coated with carbon as superior anode for sodium-ion batteries, *Small* 12 (2016) 5554–5563.
- [32] Y. Wang, R. Xiao, Y.-S. Hu, M. Avdeev, L. Chen, P2-Na0.6[Cr0.6Ti0.4]O2 cation-disordered electrode for high-rate symmetric rechargeable sodium-ion batteries, *Nat. Commun.* 6 (2015) 6954.
- [33] Q. Zhao, Y. Lu, J. Chen, Advanced organic electrode materials for rechargeable sodium-ion batteries, *Adv. Energy Mater.* 7 (2017) 1601792.
- [34] L. Zhao, J. Zhao, Y.S. Hu, H. Li, Z. Zhou, M. Armand, L. Chen, Disodium terephthalate (NA2C8H4O4) as high performance anode material for low-cost room-temperature sodium-ion battery, *Adv. Energy Mater.* 2 (2012) 962–965.
- [35] X. Wu, S. Jin, Z. Zhang, L. Jiang, L. Mu, Y.-S. Hu, H. Li, X. Chen, M. Armand, L. Chen, X. Huang, Unraveling the storage mechanism in organic carbonyl electrodes for sodium-ion batteries, *Sci. Adv.* 1 (2015) e1500330.
- [36] D.A. Stevens, J.R. Dahn, High capacity anode materials for rechargeable sodium-ion batteries, *J. Electrochem. Soc.* 147 (2000) 1271.
- [37] D.A. Stevens, J.R. Dahn, An in situ small-angle X-ray scattering study of sodium insertion into a nanoporous carbon anode material within an operating electrochemical cell, *J. Electrochem. Soc.* 147 (2000) 4428.
- [38] A. Ponrouch, A.R. Goñi, M.R. Palacin, High capacity hard carbon anodes for sodium ion batteries in additive free electrolyte, *Electrochem. Commun.* 27 (2013) 85–88.
- [39] Y. Cao, L. Xiao, M.L. Sushko, W. Wang, B. Schwenzer, J. Xiao, Z. Nie, L.V. Saraf, Z. Yang, J. Liu, Sodium ion insertion in hollow carbon nanowires for battery applications, *Nano Lett.* 12 (2012) 3783–3787.
- [40] Y. Li, S. Xu, X. Wu, J. Yu, Y. Wang, Y.-S. Hu, H. Li, L. Chen, X. Huang, Amorphous monodispersed hard carbon micro-spherules derived from biomass as a high performance negative electrode material for sodium-ion batteries, *J. Mater. Chem.* 3 (2015) 71–77.
- [41] Y. Li, Y.-S. Hu, H. Li, L. Chen, X. Huang, A superior low-cost amorphous carbon anode made from pitch and lignin for sodium-ion batteries, *J. Mater. Chem. A* 4 (2016) 96–104.
- [42] Q. Jiang, Z. Zhang, S. Yin, Z. Guo, S. Wang, C. Feng, Biomass carbon micro/nanostructures derived from ramie fibers and corncobs as anode materials for lithium-ion and sodium-ion batteries, *Appl. Surf. Sci.* 379 (2016) 73–82.

- [43] C. Bommier, T.W. Surta, M. Dolgos, X. Ji, New Mechanistic Insights on Na-Ion Storage in Nongraphitizable Carbon, *Nano Lett.* 15 (2015) 5888–5892.
- [44] S.W. Zhang, W. Lv, C. Luo, C.H. You, J. Zhang, Z.Z. Pan, F.Y. Kang, Q.H. Yang, Commercial carbon molecular sieves as a high performance anode for sodium-ion batteries, *Energy Storage Mater.* 3 (2016) 18–23.
- [45] L. Qie, W. Chen, X. Xiong, C. Hu, F. Zou, P. Hu, Y. Huang, Sulfur-doped carbon with enlarged interlayer distance as a high-performance anode material for sodium-ion batteries, *Adv. Sci.* 2 (2015) 1500195.
- [46] J. Ding, H. Wang, Z. Li, K. Cui, D. Karpuzov, X. Tan, A. Kohandehghan, D. Mitlin, Peanut shell hybrid sodium ion capacitor with extreme energypower rivals lithium ion capacitors, *Energy Environ. Sci.* 8 (2015) 941–955.
- [47] L. Fu, K. Tang, K. Song, P.A. van Aken, Y. Yu, J. Maier, Nitrogen doped porous carbon fibres as anode materials for sodium ion batteries with excellent rate performance, *Nanoscale* 6 (2014) 1384–1389.
- [48] T. Chen, L. Pan, T. Lu, C. Fu, D.H.C. Chua, Z. Sun, Fast synthesis of carbon microspheres via a microwave-assisted reaction for sodium ion batteries, *J. Mater. Chem. A* 2 (2014) 1263–1267.
- [49] Y. Li, Y.-S.S. Hu, M.-M.M. Titirici, L. Chen, X. Huang, Hard carbon microtubes made from renewable cotton as high-performance anode material for sodium-ion batteries, *Adv. Energy Mater.* 6 (2016) 1600659.
- [50] Z. Wang, L. Qie, L. Yuan, W. Zhang, X. Hu, Y. Huang, Functionalized N-doped interconnected carbon nanofibers as an anode material for sodium-ion storage with excellent performance, *Carbon N. Y.* 55 (2013) 328–334.
- [51] Y.S. Yun, K.Y. Park, B. Lee, S.Y. Cho, Y.U. Park, S.J. Hong, B.H. Kim, H. Gwon, H. Kim, S. Lee, Y.W. Park, H.J. Jin, K. Kang, Sodium-ion storage in pyroprotein-based carbon nanoplates, *Adv. Mater.* 27 (2015) 6914–6921.
- [52] H. Zhu, F. Shen, W. Luo, S. Zhu, M. Zhao, B. Natarajan, J. Dai, L. Zhou, X. Ji, R.S. Yassar, T. Li, L. Hu, Low temperature carbonization of cellulose nanocrystals for high performance carbon anode of sodium-ion batteries, *Nano Energy* 33 (2017) 37–44.
- [53] S. Zhang, K. Zhao, T. Zhu, J. Li, Electrochemomechanical degradation of high-capacity battery electrode materials, *Prog. Mater. Sci.* 89 (2017) 479–521.
- [54] J. Kasnatscheew, M. Evertz, B. Streipert, R. Wagner, R. Kl?psch, B. Vortmann, H. Hahn, S. Nowak, M. Amereller, A.-C. Gentschev, P. Lamp, M. Winter, The truth about the 1st cycle Coulombic efficiency of LiNi 1/3 Co 1/3 Mn 1/3 O 2 (NCM) cathodes, *Phys. Chem. Chem. Phys.* 18 (2016) 3956–3965.
- [55] J. Kasnatscheew, M. Evertz, B. Streipert, R. Wagner, S. Nowak, I.C. Laskovic, M. Winter, Changing established belief on capacity fade mechanisms: thorough investigation of LiNi1/3Co1/3Mn1/3O2 (NCM111) under high voltage conditions, *J. Phys. Chem. C* 121 (2017) 1521–1529.
- [56] K.-H. Chen, K.N. Wood, E. Kazyak, W.S. LePage, A.L. Davis, A.J. Sanchez, N.P. Dasgupta, Dead lithium: mass transport effects on voltage, capacity, and failure of lithium metal anodes, *J. Mater. Chem. A* 5 (2017) 11671–11681.
- [57] Y. Li, Y.S. Hu, X. Qi, X. Rong, H. Li, X. Huang, L. Chen, Advanced sodium-ion batteries using superior low cost pyrolyzed anthracite anode: towards practical applications, *Energy Storage Mater.* 5 (2016) 191–197.
- [58] Y. Li, L. Mu, Y.S. Hu, H. Li, L. Chen, X. Huang, Pitch-derived amorphous carbon as high performance anode for sodium-ion batteries, *Energy Storage Mater.* 2 (2016) 139–145.
- [59] A. Ahmadpour, D. Do, The preparation of activated carbon from macadamia nutshell by chemical activation, *Carbon N. Y.* 35 (1997) 1723–1732.
- [60] B. Zhang, C.M. Ghimbeu, C. Laberty, C. Vix-Guterl, J.M. Tarascon, Correlation between microstructure and Na storage behavior in hard carbon, *Adv. Energy Mater.* 6 (2016) 1501588.
- [61] P.-c. Tsai, S.-C. Chung, S.-k. Lin, A. Yamada, Ab initio study of sodium intercalation into disordered carbon, *J. Mater. Chem. A* 3 (2015) 9763–9768.
- [62] J. Zhang, D.-W. Wang, W. Lv, S. Zhang, Q. Liang, D. Zheng, F. Kang, Q.-H. Yang, Achieving superb sodium storage performance on carbon anodes through an ether-derived solid electrolyte interphase, *Energy Environ. Sci.* 10 (2017) 370–376.
- [63] X. Bi, X. Ren, Z. Huang, M. Yu, E. Kreidler, Y. Wu, Investigating dendrites and side reactions in sodiumoxygen batteries for improved cycle lives, *Chem. Commun.* 51 (2015) 7665–7668.
- [64] A. Kushima, K.P. So, C. Su, P. Bai, N. Kuriyama, T. Maebashi, Y. Fujiwara, M.Z. Bazant, J. Li, Liquid cell transmission electron microscopy observation of lithium metal growth and dissolution: root growth, dead lithium and lithium flotsams, *Nano Energy* 32 (2017) 271–279.
- [65] N. Sun, H. Liu, B. Xu, Facile synthesis of high performance hard carbon anode materials for sodium ion batteries, *J. Mater. Chem. A* 3 (2015) 20560–20566.
- [66] E.J. Berg, C. Villeveille, D. Streich, S. Trabesinger, P. Novák, Rechargeable batteries: grasping for the limits of chemistry, *J. Electrochem. Soc.* 162 (2015) A2468–A2475.
- [67] R. Dugas, A. Ponrouch, G. Gachot, R. David, M.R. Palacin, J.M. Tarascon, Na reactivity toward carbonate-based electrolytes: the effect of FEC as additive, *J. Electrochem. Soc.* 163 (2016) A2333–A2339.
- [68] Y. Jin, S. Li, A. Kushima, X. Zheng, Y. Sun, J. Xie, J. Sun, W. Xue, G. Zhou, J. Wu, F. Shi, R. Zhang, Z. Zhu, K. So, Y. Cui, J. Li, Self-healing SEI enables full-cell cycling of a silicon-majority anode with a coulombic efficiency exceeding 99.9%, *Energy Environ. Sci.* 10 (2017) 580–592.



Yuheng Zheng received his M.Sc. degree in the School of Energy and Power Engineering from Xi'an Jiaotong University in 2010 and he is currently working toward a Ph.D. degree in Material Science at Xi'an Jiaotong University. He has focused on low cost and long-life electrode materials for sodium-ion batteries.



Yuesheng Wang is a Postdoc at Hydro Quebec working with Prof. Karim Zaghib, Canada. He received his Ph.D. from the Institute of Physics, Chinese Academy of Sciences in 2016 while working with Prof. Yong-Sheng Hu. His recent research interests include developing and exploring novel materials for low-cost energy storage devices such as aqueous lithium or sodium ion batteries and advanced electrode material characterizations.



Yaxiang Lu received her Ph.D. degree in University of Birmingham (UK), and then she moved to University of Surrey (UK) to work as the research fellow. After that she is awarded the "International Young Scientist Fellowship" by the Institute of Physics, Chinese Academy of Sciences to work in the Key Laboratory for Renewable Energy under the supervision of Prof. Yongsheng Hu. Her research interests focus on advanced materials for energy storage and conversion, such as noble metal based electrodes for polymer electrolyte fuel cells and carbon materials for sodium ion batteries.



Dr. Yong-Sheng Hu is a professor at the Institute of Physics, Chinese Academy of Sciences. His current research interests include advanced materials for long-life and low-cost rechargeable batteries and their energy storage mechanism, particularly focusing on sodium based rechargeable batteries. He was selected as a Thomson Reuters Highly Cited Researchers in the field of Materials Science in 2014, 2015 and 2016. He also received several awards and honors, such as The 14th China Youth Science and Technology Award, Tajima Prize, Fellow of The Institute of Physics (UK), Fellow of The Royal Society of Chemistry, etc.



Dr. Ju Li is BEA Professor of Nuclear Science and Engineering and Professor of Materials Science and Engineering at MIT. His group (<http://Li.mit.edu>) performs computational and experimental research on mechanical properties of materials, and energy storage and conversion. Ju is a recipient of the 2005 Presidential Early Career Award for Scientists and Engineers, 2006 MRS Outstanding Young Investigator Award, and 2007 TR35 award from Technology Review magazine. Ju was elected Fellow of the American Physical Society in 2014 and Fellow of the Materials Research Society in 2017.